THE JOURNAL OF PHYSICAL CHEMISTRY C

Article

Cite This: J. Phys. Chem. C 2018, 122, 6593−6601

pubs.acs.org/JPCC

Phosphorus and Nitrogen Centers in Doped Graphene and Carbon Nanotubes Analyzed through Solid-State NMR

Adam R. MacIntosh,[†] Gaopeng Jiang,[§] Pouyan Zamani,[§] Zhongxin Song,[‡] Adam Riese,[‡] Kristopher J. Harris,[†] Xiaogang Fu,[§] Zhongwei Chen,[§] Xueliang Sun,[‡] and Gillian R. Goward[†,*]

[†]Department of Chemistry and Chemical Biology, McMaster University, 1280 Main Street West, Hamilton, Ontario L8S 4L8, Canada

[‡]Faculty of Engineering, The University of Western Ontario, 1151 Richmond Street, London, Ontario N6A 5B9, Canada

[§]Department of Chemical Engineering, University of Waterloo, 200 University Avenue West, Waterloo, Ontario N2L 3G1, Canada

Supporting Information

ABSTRACT: Graphene and carbon nanotubes (CNTs) have been investigated closely in recent years because of their apparent positive effect on the electrochemical performance of new fuel cell and battery systems as catalyst stabilizers, supports, or metal-free catalysts. This is particularly true for doped graphene and CNTs, where only a small amount of doping with nitrogen and/or phosphorus can have a remarkable effect on the material performance. A direct link between structure and function in these materials is, as of yet, unclear. Doped graphene and CNTs were synthesized using varied chemical vapor deposition-based methods, and ssNMR was used to unambiguously identify dopant atom sites, revealing that these particular synthesis methods result in highly homogeneous populations of installed phosphorus and nitrogen atoms. We present the first experimental ^{15}N spectrum for graphitic nitrogen in N-doped graphene. ^{15}N-labeled nitrogen-doped graphene synthesized as reported here produces mainly graphitic nitrogen sites located on the edges of sheets and around defect sites. $^{1}H-^{1}H$ and $^{1}H-^{15}N$ correlations were also used to probe dopant nitrogen sites in labeled and unlabeled N-doped graphene. A nearly homogeneous population of phosphorus in P-doped graphene is found, with an overwhelming majority of graphitic phosphorus and a small amount of phosphate oligomer. Similar findings are noted for the phosphorus sites in phosphorus and nitrogen codoped CNTs with a minor change in chemical shift, as would be expected from two chemically similar phosphorus sites in carbon allotropes (CNTs vs graphene sheets) with significantly different electronic structures.

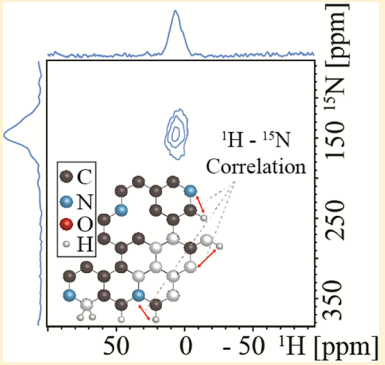

INTRODUCTION

Fuel cells and high-density batteries have been under intense investigation in recent years and are well-positioned to become ubiquitous in the auto transportation, aviation, and bulk power storage industries. When fuelled or charged with energy from a green renewable source, these devices represent half of the solution to the world's energy problem, the other half being the collection of energy from renewable sources (solar, geothermal, wind, tidal, etc.).[1−5] An unfortunate drawback of these devices is the necessity of noble metals (commonly platinum, iridium, and palladium) to catalyze the electrochemical reactions to convert chemical energy from hydrogen into electricity. Even with the increasingly present economic and political impetus for new energy storage and distribution systems, these devices would benefit greatly from seeing a reduced or removed dependence on noble metals.[6−10]

The use of doped graphitic materials [i.e., graphene and carbon nanotubes (CNTs)] has been shown in recent publications to reduce the dependence on precious metals for catalysis. Both nitrogen- and phosphorus-doped carbons can be used as metal-free catalysts toward the oxygen reduction reaction and exhibit outstanding catalytic activity and durability in alkaline media.[11−14] Significant differences in electrochemical activity are found between doped and undoped carbons, which has been attributed to the changes in energy gaps in the band structure of these materials brought on by doping, despite the loading levels of as little as 0.5% by weight.[15−18]

Although the bulk electrochemical and physical properties of doped carbon materials are relatively simple to study, the nonstoichiometric and poorly ordered nature of these structures make the collection of meaningful data on the micro- to nanoscopic scale challenging. To understand the nature of these doped carbon materials, a clear picture of the chemical environment around dopant sites must be drawn, and hence a structural analysis method with high resolution and high specificity is necessary. Most structural analyses of these materials are based on X-ray spectro-microscopies, particularly energy-dispersive X-ray (EDX) spectroscopy and electron microscopy. Scanning electron microscopy and transmission electron microscopy (SEM and TEM) can be used to get an idea of any bulk morphological changes doping may have on sheets and tubes, and EDX can provide surface elemental

Received: November 27, 2017
Revised: February 16, 2018
Published: February 18, 2018

DOI: 10.1021/acs.jpcc.7b11671
J. Phys. Chem. C 2018, 122, 6593−6601

composition with micron-level spatial resolution, but even with these data in hand, it can be difficult to link structure and function in these materials in a chemically meaningful way.

Solid-state nuclear magnetic resonance (ssNMR) spectroscopy is an ideal analysis method because of its extreme sensitivity toward slight changes in chemical environment, despite being an inherently insensitive analytical technique. Significant analytical work has been done on nonconductive carbons, but a relatively small amount has been applied to conductive and/or doped carbon samples, including the following examples. Some of the earliest ssNMR work done on amorphous carbons was done to investigate which of the many potential models of graphene was correct. This study required careful thin-film deposition of carbon with isotopically labeled precursors; however, resolution between graphitic and other carbon sites was obtained, and a clearer picture of the structure of graphene was developed.[19] Ishii et al. synthesized graphene oxide through chemical vapor deposition using ^{13}C-labeled methane and were able to collect 2D $^{1}H-^{13}C$ correlation spectra in a reasonable experimental time, which unambiguously solved the debated structure of graphene oxide.[20] Leskes et al. have built a body of work applying ssNMR techniques to conductive and doped carbon materials, both ex and in situ, for use in battery and supercapacitor systems, recently using isotopic labeling and dynamic nuclear polarization enhancement to selectively study the solid−electrolyte interface at the surface of graphitic current collectors.[21−23] In previous work, we used various ^{1}H, ^{2}H, and ^{13}C techniques to characterize acidic functional groups covalently attached to graphene with unprecedented resolution; the recorded spectra even showed appreciable resolution between carbon atoms in a functional group aliphatic chain.[24] In addition, the surfaces of the graphenelike MXene family of layered metallic materials were successfully characterized through ssNMR, even probing the interactions between surface hydroxide and fluoride sites.[25] In a separate study, the carbon spectra of a graphene nanosheet coated with tin−graphite core−shell nanoparticles were found to be extremely sensitive to carbon density and respond to changes as the anode carbon was reduced during discharge. This ssNMR information was produced from a tiny amount of sample thanks to the use of magic-angle spinning along with the signal-enhancing Carr−Purcell−Meiboom−Gill pulse sequence.[26] However, the amorphous and inhomogeneous nature of these samples tends to produce crowded difficult-to-acquire spectra with overlapping broad signals. Furthermore, the electronic conductivity of these materials leads to a magnetically induced current within the sample which, in turn, produces a non-negligible magnetic field. The interaction of this field with the applied field can cause issues with the physical acquisition of data and can make the collection of interpretable spectra yet more challenging. As a result, part of the work described here is NMR method development, whereas the ultimate goal of this line of study is to unambiguously link catalyst stabilization or catalytic performance to specific structures, leading to the selective tuning of the electronic properties of these fascinating materials.[27−29]

In this work, we describe the ssNMR analysis of a number of doped carbon materials: nitrogen-doped graphene (NG), phosphorus-doped graphene (PG), and CNTs codoped with both phosphorus and nitrogen. ssNMR has been used successfully to analyze graphene and other amorphous carbons; however, this study will use this tool to focus on dopant sites specifically. These samples were synthesized with varying methods and precursor materials, both with and without isotopic labeling. The results shown here elucidate the chemical environments around dopant sites in graphene and CNTs, leading to a deeper understanding of the function of these materials in energy storage and delivery media. We demonstrate that ssNMR is a useful tool in the analysis of novel carbon allotropes and can provide important chemical information that is inaccessible through the usual means of SEM and EDX.

The samples studied in this work were (i) two closely related phosphorus-doped graphenes, one with a significant presence of oxygen (PG and PG-O), (ii) NG, and (iii) phosphorus/nitrogen-codoped carbon nanotubes (PNCNTs), which were synthesized by a variety of methods.

EXPERIMENTAL SECTION

Synthesis: Doped Graphenes (PG, PG-O, and NG). GO was synthesized according to the improved Hummers' method from natural graphite flakes.[30] First, 98% H_2SO_4 (360 mL) and 85% H_3PO_4 (40 mL) were mixed carefully in a round-bottom flask in an ice bath. Graphite powder (2 g) was added into the concentrated mixed acid and stirred for 1 h. Then, the strong oxidizing agent $KMnO_4$ (18 g) was added slowly into the mixture, and the oxidation reaction was kept at 50 °C for 16 h. After cooling down the mixture, the oxidation reaction was terminated. Distilled deionized (DDI) water (400 mL) and 20 mL of H_2O_2 (20 mL) were added dropwise and then stirred for 30 min. Afterward, the mixture was centrifuged and washed with DDI water, 5% HCl, and ethanol. Finally, the GO nanosheets were obtained by freeze-drying the GO suspension.

To convert GO into PG, typically 300 mg of triphenylphosphine (TPP) was first dissolved in 100 mL of isopropyl alcohol (IPA) at ambient temperature. Then, freeze-dried GO powder (60 mg) was added to the solution, and the mixture was dispersed by sonication for 2 h. After the color of the suspension changed to dark gray, the mixture was transferred onto a hot plate and IPA was evaporated overnight. The obtained solid was ground and placed in an alumina boat. Then, the mixture underwent heat treatment to 1000 °C with a ramp of 10 °C min^{-1} under an atmosphere of Ar. The temperature was maintained at 1000 °C for 30 min under Ar and another 30 min under 10% H_2/Ar. PG was collected after this treatment.

A second sample, synthesized via the same method as noted above but with the final heating done in a pure Ar atmosphere (i.e., without H_2 gas), produced a PG with significantly higher amounts of oxygen than in the original synthesis. This "oxygen-rich" PG will be referred to as PG-O.

For NG, a synthesis based on the pyrolysis of polyaniline was employed. ^{15}N-labeled aniline (3 g), iron(III) chloride ($FeCl_3$, 30 mg), ammonium peroxydisulfate (6.8 g), and a carbon source (CNTs, 400 mg) were added sequentially to a hydrochloric acid solution. These components in solution acted as a nitrogen source precursor, catalyst, oxidizer, and carbon source, respectively. The mixtures were vigorously stirred at room temperature for 48 h to allow full polymerization of the aniline into polyaniline. After 2 days, the liquid was evaporated, and the solid polymer was assembled. This precursor was then pyrolyzed at 200 °C and later at 900 °C for 1 h using a 30 °C min^{-1} heating rate under an argon atmosphere. The solid carbonized materials were then leached in sulfuric acid at 80−90 °C to remove the remaining iron

DOI: 10.1021/acs.jpcc.7b11671
J. Phys. Chem. C 2018, 122, 6593−6601

complexes as well as to introduce porosity. After this leaching step, the material was heat-treated at 900 °C in argon for 3 h. At this point, the sample is referred to as NG. Where noted, treatment in ammonia gas was then performed at 900° for 15 min.

Synthesis: Doped Carbon Nanotubes (PNCNTs). PNCNTs were prepared via the floating-catalyst chemical vapor deposition (CVD) method using ferrocene (98%, Aldrich) as the catalyst with TPP (99%, Sigma) and imidazole (99%, Sigma) as the P and N sources, respectively. Both precursors also provided the carbon for CNT growth. A mixture of imidazole and 2.5 wt % TPP (2 g total) was placed in a small quartz crucible. Ferrocene (20 mg) was placed in a small holder, separate from the precursors, on the quartz crucible. A substrate alumina crucible was placed in the center of a quartz tube in a tube furnace. The precursor and catalyst crucibles were placed near the opening of the furnace, and Ar gas was flowed through the tube for 20 min to remove air. The temperature was raised to 850 °C, at which point the ferrocene and the precursors were evaporated and transferred to the substrate by the Ar flow. The substrates were kept at the set temperature for 10 min and then cooled to ambient temperature under Ar.

Characterization. The morphology and surface elemental analysis of PG and NG samples were examined by SEM (LEO 1530) and X-ray photoelectron spectroscopy (XPS) (Thermo Scientific, Al Kα X-ray source). The morphology and structure of the PNCNTs were studied using a Hitachi S-4800 field-emission scanning electron microscope and a JEOL 2010F transmission electron microscope. Chemical compositions of PNCNTs were investigated by XPS using a Kratos Axis Ultra spectrometer. XPS data were interpreted using the NIST XPS database.[31] A summary of these elemental analyses can be found in Table 1.

Table 1. Summary of Elemental Analyses via XPS Survey

sample	carbon (at. %)	nitrogen (at. %)	oxygen (at. %)	phosphorus (at. %)
PG	98.74		0.03	1.26
PG-O	96.01		3.39	0.60
NG	91.40	4.07	4.26	
PNCNTs	88.7	6.2	3.8	1.1

ssNMR spectra were collected on Bruker AVANCE 300, 500, and 850 MHz spectrometers using 1.9, 2.5, or 4 mm MAS rotors. Where samples were conductive enough to cause difficulty with spinning the rotors or tuning/matching the probe, dilution with Teflon powder was used (up to 5:1 by the mass of Teflon/sample), the Teflon having been found to produce no interfering ^{1}H or ^{31}P signals under the experimental conditions employed (see Figure S1). ^{1}H and ^{13}C spectra were referenced to adamantane at 1.85 and 38.5 ppm (high-frequency peaks), respectively. ^{31}P spectra were referenced to 1 M phosphoric acid at 1 ppm, and ^{15}N spectra were referenced to glycine−HCl at 33.9 ppm (on the unified ^{15}N chemical shift scale proposed by Bertani et al.).[32] Typically, hard pulses were calibrated to produce a nutation frequency of 62.5 kHz, and where necessary, 50 kHz of two-pulse phase-modulated (tppm) ^{1}H decoupling was found to sufficiently remove unwanted homo- or heteronuclear coupling. For Hahn echo experiments, echo periods were set to 2 rotor periods or between 33 and 66 μs depending on the MAS rate. ^{1}H → ^{15}N cross-polarization (CP) experiments optimized for signal intensity used a contact time of 3 ms. ^{1}H → ^{15}N dipolar heteronuclear multiple quantum coherence (D-HMQC) experiments used a recoupling time of 200 μs. Typical recycle delays for these experiments were 4 s for ^{1}H, 10 s for ^{15}N, and 2 s for ^{31}P; however, delays ranging from 0.2 to 500 s were used to identify species with unusual relaxation times.

RESULTS AND DISCUSSION

Part 1: Phosphorus-Doped Graphene (PG and PG-O). Both PG and PG-O demonstrate a typical graphitic sheet-like morphology in the SEM images seen in Figure 1. EDX analysis

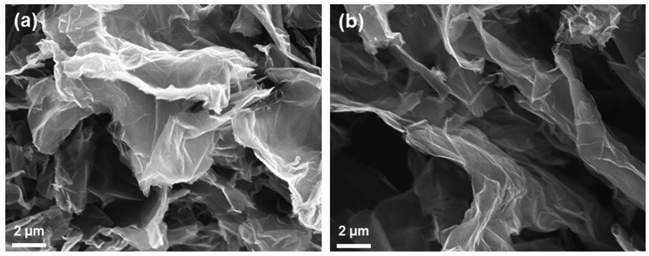

Figure 1. SEM images of PG-O (a) and PG (b).

does not show a detectable presence of oxygen in PG and shows that more phosphorus atoms are present in PG compared to PG-O, as is seen in Table 1. High-resolution XPS spectra of the P 2p edge for both of these samples are shown in Figure 2. These spectra have a markedly low signal-to-noise ratio (SNR), likely because of the low level of elemental doping in these samples. Given the poor signal intensity and resolution, there is a significant uncertainty in the binding energies and relative amounts of each species, but a tentative signal assignment is as follows: elemental phosphorous (~129.6 eV), graphitic phosphorous (~131 eV), and oxidized graphitic phosphorous (~132.5 eV). The splitting of the simulated peaks (shown as solid and dashed lines) results from taking into account the orbital splitting between $2p_{3/2}$ and $2p_{1/2}$ states. Interestingly, the XPS spectrum of PG-O also includes intensity at energies consistent with a high-oxidation-state phosphorous species, such as phosphorus pentoxide (P_2O_5) and/or orthophosphoric acid (H_3PO_4), which could be attributed to the spontaneous reactions of existing white phosphorous under exposure to air and humidity. The proportion of the two oxygen-free P species (elemental and graphitic) in PG is higher than that of PG-O (79 vs 69% of the total signal), indicating that the reductive environment created by hydrogen at 1000 °C purifies the sample and removes any residual high-oxidation-state phosphorous species in PG.

ssNMR spectroscopy is introduced as a method of refining the XPS data given that the resolution is likely to be better in many cases, there are various spectral-editing tools, and the technique reports on the overall composition of the sample rather than just the surface. ^{31}P Hahn echo spectra for PG and PG-O are shown in Figure 3. The spectra are dominated by a similar feature: a ca. 45 kHz broad resonance centered at about 150 ppm for PG-O and 75 ppm for PG. The breadth of this peak is attributed to a wide array of sites with slightly different isotropic chemical shifts, reflecting the broad array of environments expected to be found in the graphitic sheet, and represents "graphitic" phosphorus, bonded to three sp^2-hybridized carbon atoms. The ^{31}P Hahn echo spectrum of PG

DOI: 10.1021/acs.jpcc.7b11671
J. Phys. Chem. C 2018, 122, 6593−6601

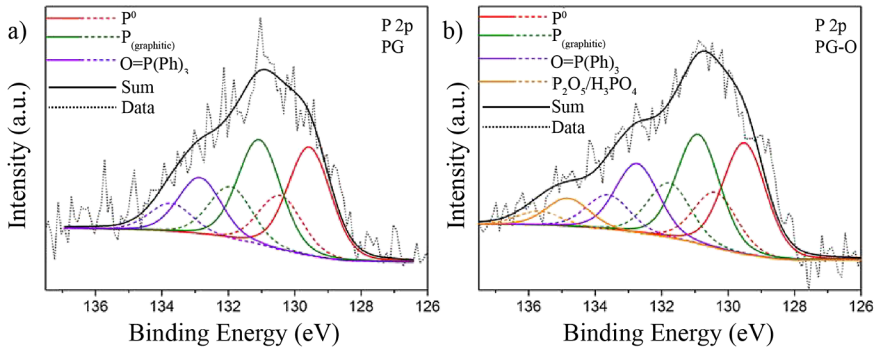

Figure 2. High-resolution P 2p edge XPS spectra for PG (a) and PG-O (b).

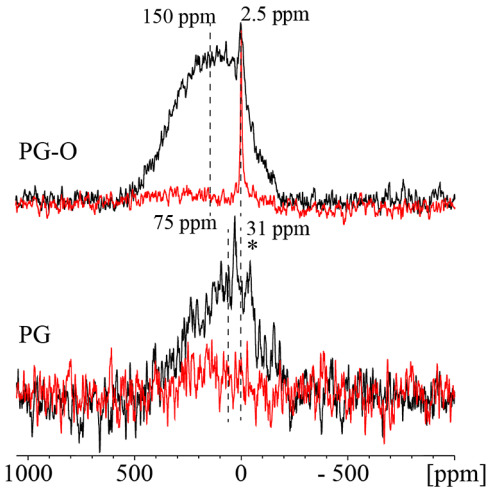

Figure 3. ^{31}P Hahn echo (black) and ^{1}H → ^{31}P CPMAS Hahn echo (red) ssNMR spectra of PG-O and PG, collected at 7.0 T at an MAS rate of 20 kHz (23.5 ppm on this scale). Asterisks denote spinning sidebands. CPMAS signal intensity indicates phosphorus sites near in space to protons.

shows a weaker signal for the same number of scans compared to PG-O (because of an increased amount of insulating Teflon powder to facilitate data acquisition) but likely reflects graphitic P atoms equivalent to those observed in PG.

The narrower peaks seen in the 30−0 ppm range in both spectra in Figure 3 represent less than 2% of the total signal intensity and are likely to be caused by small amounts of side products. Peaks in this shift range generally represent polyphosphate or polyorthophosphate species at different levels of hydration.[33] ^{1}H → ^{31}P cross-polarization magic-angle spinning (CPMAS) spectra (shown in Figure 3 in red) show a signal, which matches the narrow peak in the direct spectrum, indicating a short ^{1}H−^{31}P internuclear distance and that the phosphate species in PG-O is likely either highly hydrated or a polyorthophosphate, which is consistent with the XPS data in Figure 2. The fact that little CP occurs to the extremely broad peak is consistent with its assignment as a graphitic phosphorus environment, where protons would be remote. The sharp peaks in the PG spectrum are not seen in the ^{1}H → ^{31}P CPMAS experiment, indicating a proton-deficient environment, likely caused by the removal of residual graphene-surface alcohol groups in the reductive H_2 environment introduced at the end of the synthesis. It is also possible considering the low SNR for this spectrum that these features are caused by random noise. These results highlight the complementary nature of NMR and XPS in the study of bulk and surface composition even with extremely low amounts of sample.

It should be noted that the two spectroscopies report on different locations in the sample: the XPS method is surface-sensitive, whereas NMR spectra observe the overall composition. Whereas the XPS data imply a relatively impure sample, where oxygenated and elemental phosphorous compose large parts of the spectrum, the NMR results demonstrate that past the surface, the composition is more homogeneous. This may hint at the fact that the thickness of the graphitic sheet stacks is significantly larger than the penetrative depth of the XPS analysis. There is only a few percent of oxygenated polyphosphates in the bulk material according to NMR. The exact amount of elemental phosphorous is harder to ascertain, but it is reasonable to assume that if that amount were comparable to the amount of graphitic phosphorus, the observed line shape would be broader and more asymmetric. Considering how narrow the elemental phosphorus signal is compared to the observed signal, it is estimated that the maximum elemental phosphorus content possible in the sample is 20%. ^{31}P NMR spectra of the white and black allotropes of phosphorous yield sharp, easily detected peaks in the ca. −450 to −500 ppm range, whereas the (crystalline) violet and (disordered) red allotropes yield ca. 100 ppm broad peaks at ca. 75 ppm, which would be difficult to separate from the broad graphitic phosphorous signal if present in small amounts.[34] Notably, a previous NMR study found that violet or red phosphorous NMR peaks were visible above the graphitic signature in a doped graphene.[35] The first ^{31}P NMR spectrum of a P-doped graphene was recently reported and is generally in agreement with the present study.[33] However, the previously reported material was synthesized via an alternate route, which aimed at providing much higher dopant levels but resulted in a material with orders of magnitude more impurities than the material synthesized here. The present study shows that lower dopant levels produce samples with a narrower distribution of dopant site types and that the analysis methods presented here would be useful in determining maximum doping levels. In particular, it appears to be important to use ssNMR to track the amount of oxygenated phosphorous compounds in the overall material, rather than the XPS observation of the surface composition. The benefits of a reliable synthesis method producing a homogeneous product are obvious, and analysis by both XPS and ssNMR is a key to observing and controlling the nature of these complicated materials and for implementing them in practical applications.

Part 2: Phosphorus- and Nitrogen-Doped Carbon Nanotubes. SEM and TEM images of PNCNTs are shown in

DOI: 10.1021/acs.jpcc.7b11671
J. Phys. Chem. C 2018, 122, 6593−6601

Figure 4. The length of PNCNTs from SEM is around 30 μm. The bamboolike structure, which is characteristic of PNCNTs, is clearly seen in the TEM images of the PNCNTs. Interestingly, there appear to be two types of tubes in Figure 4b, one with narrow channels and very thick walls (center and right) and the second type with wider channels (left side of the image). This phenomenon was also recently observed by Nicholls et al.[36] Furthermore, the carbon planes are not perfectly parallel and have varying interplane distances, which are greater than those of standard sp^2 carbons and likely indicate disorder in the carbon lattice caused by the presence of heteroatoms.

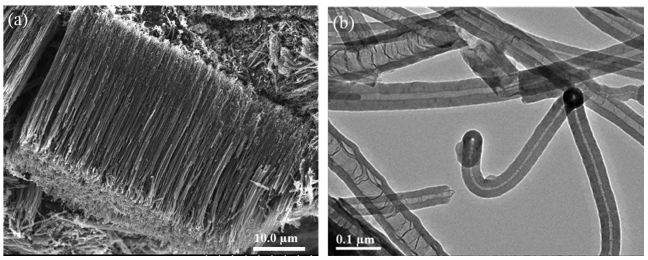

Figure 4. (a) SEM and (b) TEM of PNCNTs.

High-resolution N 1s and P 2p edge spectra for PNCNTs are shown in Figure 5. As shown in Figure 5a, there are two peaks within the N 1s signal. The peak centered at 398.1 eV corresponds to pyridinic N, and the peak at 400.8 eV corresponds to graphitic N. The graphitic-to-pyridinic nitrogen ratio determined from the XPS data is 1.8. A high-resolution P 2p peak from the PNCNT sample is shown in Figure 5b. The peak centered ~130.2 eV can be assigned to elemental phosphorus, whereas that at 132.5 eV corresponds to a graphitic phosphorus bonding environment.

Figure 6 shows a ^{31}P echo of PNCNTs, which is similar to the ^{31}P spectrum collected for PG (as can be seen in the comparison in Figure 7). One broad peak is observed, centered at 250 ppm, and is assigned to graphitic phosphorus built into the walls of the CNTs. Similarly to PG and PG-O, no white or black elemental phosphorous is present, though there may be small amount of unresolved signal from disordered elemental phosphorous obscured by the much larger graphitic phosphorus signal. In contrast to the doped graphenes, the ^{31}P NMR spectrum of PNCNTs does not support the presence of significant amounts of phosphate in the sample. Again, it should

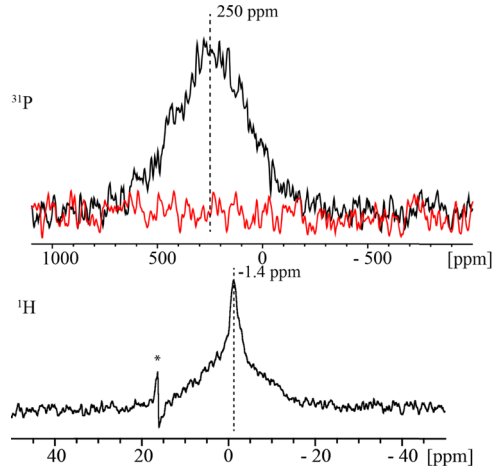

Figure 6. ^{31}P Hahn echo (black, top), ^{1}H → ^{31}P CPMAS (red), and ^{1}H Hahn echo (bottom) ssNMR spectra of PNCNTs collected at 7.4 T at an MAS rate of 20 kHz. The asterisk marks a transmitter artifact.

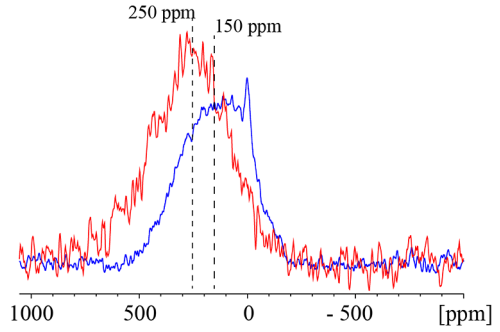

Figure 7. ^{31}P Hahn echo spectra of PG-O (blue) and PNCNTs (red). The phosphorus sites are similar, but the chemical shift is clearly affected by changes in energy gaps in the band structure.

be noted that the XPS analysis may report elemental phosphorous (or phosphate groups in the case of PG) at the surface, whereas the NMR analysis shows that there is little of these impurities across the entire bulk of the sample. Categorization of these two observations is slightly complicated by the poor resolution of the XPS spectrum. The penetrative depth of the XPS analysis is important to consider here as well. The TEM image in Figure 4 indicates that the nanotube wall thickness is roughly 20 nm, much thinner than XPS penetration

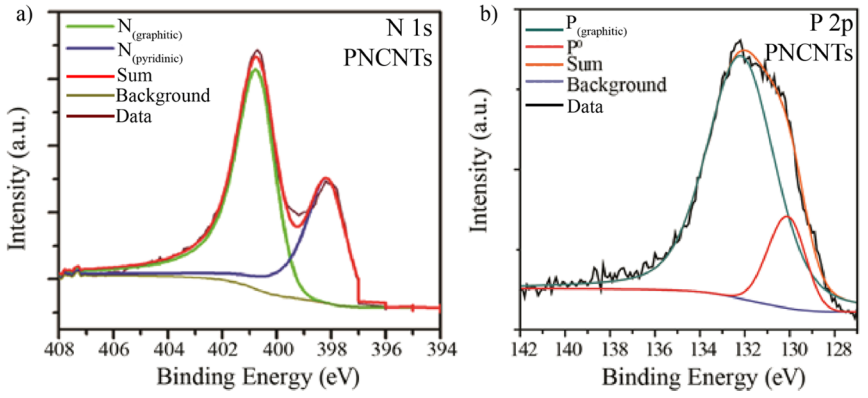

Figure 5. XPS survey spectra for PNCNTs. (a) N 1s and (b) P 2p edges. NB spin−orbital splitting in the P 2p edge spectra is accounted for, but not explicitly labeled.

DOI: 10.1021/acs.jpcc.7b11671
J. Phys. Chem. C 2018, 122, 6593−6601

(ca. micrometers). Differences between the XPS and NMR analysis may arise from XPS being unable to penetrate inside of the clusters of nanotubes seen in the SEM. It is clear that in the cases where XPS may be ambiguous, ssNMR can be used to verify any interpretations. Repeating this experiment under static conditions did not have a significant effect on the width of the signal, indicating that an array of very similar environments exists for phosphorus dopant sites (i.e., the width is caused by a distribution of similar chemical shifts).

Also, shown in Figure 6 are the ^{1}H echo and ^{1}H → ^{31}P CPMAS spectra of PNCNTs. An unusually weak ^{1}H signal in this material, coupled with the negative ppm shift seen in the main narrow peak at −1.4 ppm, indicates that this signal is caused by a small amount of (likely ambient) water adsorbed onto the CNT surfaces, shifted due to interactions with the ring currents of circulating π-electrons.[37−39] The broader signal spanning from 10 to −10 ppm may be caused by carbon-bonded protons at the edges of nanotubes or residual probe background. The lack of any signal in the CP spectrum, tested at contact times ranging from 1 to 9 ms, indicates that whatever protons are present are not near in space to the tube-wall phosphorus site (cf. NG below).

Perhaps, most importantly, there is a difference in ^{31}P chemical shift between the dopant sites in the nanotubes and graphene sheets (see Figure 7). This difference is likely related to the differences in the electronic structure between the two materials because of the well-known relationship between empty and full orbital energy spacing and the NMR chemical shift.[40] The presence of an electronic structure analogous to that of a small band-gap semiconductor or conductive metal is hinted at by rapid ^{31}P spin−lattice (T_1) and spin−spin (T_2) relaxation rates, with rate constants on the order of a few milliseconds in both PNCNTs and PG. There was no evidence of significant T_2 variations across the line shapes while employing microsecond-scale echo times in the Hahn echo experiment, adding further evidence that their breadth is caused by variations in the isotropic chemical shift. These findings further demonstrate that the P dopant atoms are directly connected with the carbon materials, as there must be some source of fluctuating magnetic field (in this case, conducting electrons) to induce ^{31}P relaxation rates that are much faster than those found in insulating, diamagnetic materials. The apparent sensitivity of NMR to the electronic structure, via chemical shift changes and relaxation rates, suggests that this technique is well-suited to the study of carbon materials doped for catalytic applications, as this behavior is undoubtedly related to the shape of the energy gaps in the band structure.

Part 3: NG. Figure 8 shows an SEM image of NG displaying the expected sheetlike graphene morphology. The N 1s edge high-resolution XPS spectra of NG before and after treatment in ammonia are shown in Figure 9, apparently displaying peaks corresponding to graphitic (401.5 eV) and pyridinic (398.7 eV) nitrogen sites. The spectra are also consistent with the presence of some pyrollic (400.2 eV) sites, though the resolution makes this difficult to ascertain. Disregarding these potential sites, it seems that ammonia treatment increases the intensity of nitrogen signals for pyridinic and graphitic nitrogen. The graphitic-to-pyridinic nitrogen ratios for the samples before and after ammonia step were 1.2 and 1.8, respectively. Interestingly, the ratio of graphitic-to-pyridinic nitrogen is higher in the PNCNTs (1.8) before ammonia treatment (see Figure 5b), which suggests that the presence of P may play a role in promoting the formation of graphitic nitrogen species during doping.

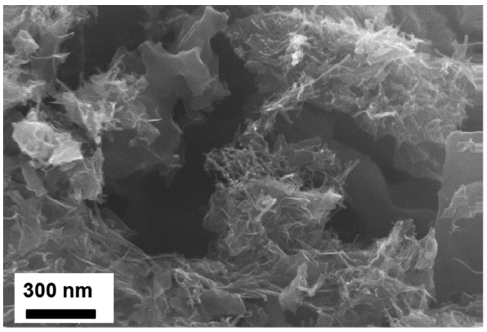

Figure 8. SEM image of NG.

Figure 10 shows a ^{15}N Hahn echo NMR spectrum of ^{15}N-labeled NG (the NMR sample was not treated with ammonia). The spectrum displays two main features: a tall narrower peak centered at about 172 ppm and a broad feature spanning from 375 to 220 ppm at a ratio of about 1.3:1. A ^{15}N spectrum of graphene made by chemical reduction of graphene oxide with ^{15}N-labeled hydrazine has been reported by Ruoff et al. and shows a single nitrogen site at roughly 190 ppm. This resonance was attributed to edge-based pyrazole groups generated during the reduction process, as a side product of the chemical reduction of graphene oxide with hydrazine originally intended to produce graphene sheets.[41] The ^{15}N chemical shifts observed in the material presented here are different than those observed by Ruoff et al., and the chemical environments are therefore quite different than the edge-terminating pyrazole groups. Also shown in Figure 10 is a ^{1}H Hahn-echo NMR spectrum of NG including background suppression. Two sites are immediately apparent: at 0 and −2.7 ppm. The 7.2 ppm peak observed via D-HMQC is obscured by the 6.5 ppm peak because of the residual probe background (confirmed via a probe background measurement which contained this signal; see Figure S2), only visible due to the low amount of ^{1}H signal. The low-frequency peaks can be amplified or attenuated through humidification and dehumidification, and hence they are assigned to water molecules which are adsorbed onto the graphitic sheets under the influence of a ring-current shift to lower-than-expected chemical shifts.[37,42]

A ^{1}H−^{15}N D-HMQC NMR spectrum, shown in Figure 11a, was collected to probe the existence of correlations between proton and nitrogen sites.[43] In broad terms, any correlation between ^{1}H and ^{15}N sites indicates that these sites are near in space to one another and may be bonded together. The only correlation evident from this 2D spectrum links together a ^{15}N site at 145.7 ppm with a ^{1}H site at 7.2 ppm. The heteronuclear correlation experiment reveals that there are actually two ^{15}N resonances in the 120−200 ppm region: one from a site that is near a proton and one from a site that is not. Figure 11b illustrates this point and further confirms it via comparison of direct and two proton-correlated ^{15}N NMR spectra (slice of 2D HMQC and 1D ^{1}H−^{15}N CP). Only the direct ^{15}N spectrum is quantitative, and hence this low-frequency proton-correlated peak is likely present at a smaller amount than the other two sites. It is also possible that polarization transfer from protons to the high-frequency site nitrogen nuclei is limited by rapid relaxation of the spin-locked or transverse magnetization, but clearly there is a strong correlation between structural protons and the low-frequency nitrogen site.

DOI: 10.1021/acs.jpcc.7b11671
J. Phys. Chem. C 2018, 122, 6593−6601

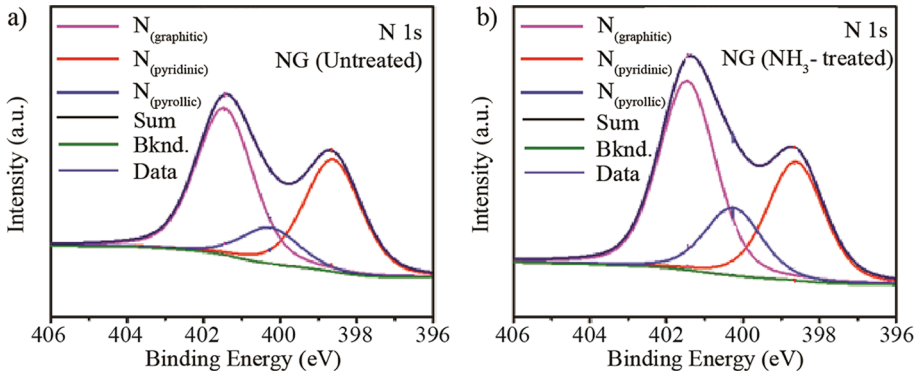

Figure 9. N 1s edge XPS spectra of NG before (a) and after (b) high-temperature treatment with ammonia.

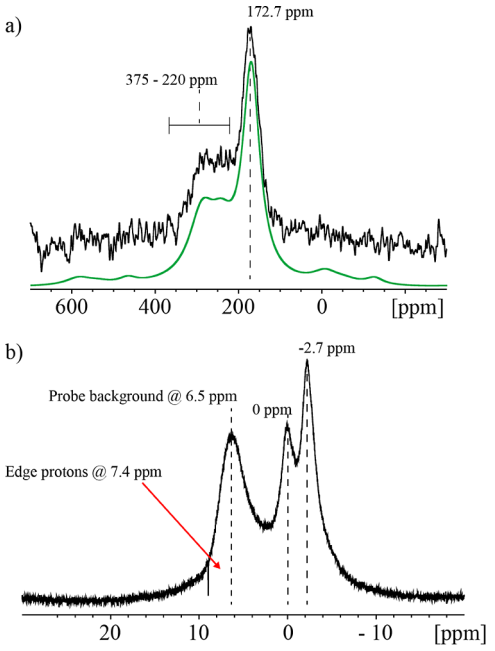

Figure 10. (a) ^{15}N Hahn echo (three-site sum of deconvolution in green) and (b) ^{1}H Hahn echo ssNMR spectra of ^{15}N-labeled NG collected at 11.7 T at an MAS rate of 15 kHz.

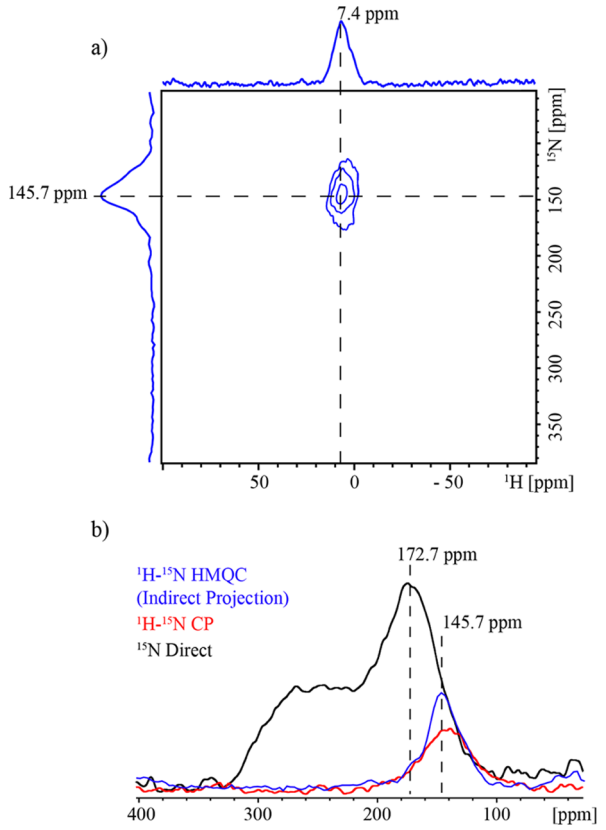

Figure 11. (a) ^{1}H−^{15}N D-HMQC 2D ssNMR spectrum of NG collected at 11.7 T at an MAS rate of 20 kHz. (b) ^{15}N Hahn echo and ^{1}H−^{15}N CP (both collected at 19.9 T at MAS rates of 30 and 15 kHz, respectively) spectra of NG compared with the indirect projection of a ^{1}H−^{15}N 2D D-HMQC ssNMR spectrum.

A recent study by Wang et al. investigated the likely ^{15}N chemical shifts for graphitic nitrogen via a first-principles computational analysis.[44] Their analysis was modeled as a single relaxed (i.e., geometry optimized) graphene sheet in a vacuum and was sensitive to the changes in chemical and electronic environment introduced by defects. Comparing this experimental data to the computational analysis by Wang et al., the high-frequency feature is assigned to pyridine-like nitrogen centers localized mainly along the zigzag and armchair edges of graphene sheets bonded to aprotic sp^2-hybridized carbons.[44] In particular, pyridinic sites near vacancy defects in the sheet satisfy both the chemical shift and the aprotic environment, consistent with the NMR spectrum. The proton-correlated nitrogen centers of the 145.7 ppm peak are in excellent agreement with calculated chemical shifts for $z^{\text{edge-1}}$ nitrogen sites, which bridge two carbon rings at the sheet edges (where the nearby sheet edge necessitates C−H or C−OH termination groups that supply the N,H proximity observed via NMR).[45] Without ^{15}N−^{1}H correlation experiments, the peak at 172 ppm might be erroneously assigned to a variety of protonated sites whose calculated chemical shifts are in approximate agreement. The nearest aprotic match sites are graphitic, either replacing a carbon atom in the normal graphene sheet or as part of a Stone−Wales or vacancy defects.[45] Finally, we note that more distant ^{15}N chemical shifts predicted for pyrrolic sites imply that there is no significant amount of such environments present. However, the poor resolution of the surface-sensing XPS spectrum in that region prevents definitive conclusions about whether such sites are present at the surface despite contributing little to the overall composition. Additionally, we note that, to our knowledge, this is the first reported NMR observation of graphitic nitrogen sites, as opposed to edge-terminating pyrazole groups.[41] An illustrated N-doped

DOI: 10.1021/acs.jpcc.7b11671
J. Phys. Chem. C 2018, 122, 6593−6601

graphene sheet highlighting the N-dopant sites observed in this study is presented in Figure 12.

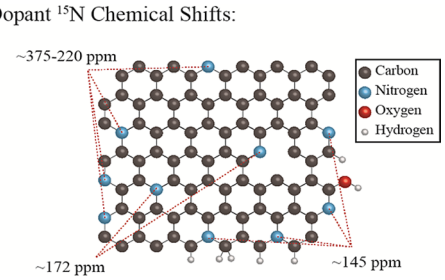

Figure 12. Illustration of a hypothetical graphene sheet with the nitrogen centers elucidated in this study. The chemical shifts of dopant nitrogen atoms are effected by nearby dopant sites because of electronic structure changes, and hence this particular sheet only serves illustrative purposes. Unnecessary protons are omitted.

Our ^{15}N results on NG show that this synthesis method produces relatively homogeneous N sites, that is, roughly equal amounts of graphitic and pyridinic sites. This ssNMR result correlates with the XPS analysis in Figure 9, though there is less resolution evident in XPS. The relationship between atomic structure and function can now be probed directly without worrying about side reactions and inactive or counteractive dopant sites. If there is a relationship between catalytic activity and site distribution, ssNMR is shown to be a valuable tool in discovering and probing it.

CONCLUSIONS

The chemical environment of dopant atoms in graphene sheets has been experimentally probed through ssNMR and XPS. A CVD-based method using TPP as the phosphorus and carbon source produces homogeneous graphitic phosphorus sites with a high degree of specificity. Mechanisms of doping and physical behavior of this material, especially when compared to graphene, can be made reliably with this model. Similarly, a CVD method with aniline as the precursor produced graphene doped with a roughly equal proportion of edge-based and defect-based N sites. To our knowledge, this is the first reported experimental ^{15}N ssNMR spectrum of NG, and it matches recently published simulations data well. The P and N sites of a polydoped CNT sample were also studied. ^{31}P spectroscopy resembles that found in PG, with a downfield shift likely attributable to the difference in electronic structure between these materials. It is shown that the application of the extreme sensitivity and selectivity of ssNMR to the study of modified graphitic materials is a challenging but revealing method of analysis.

ASSOCIATED CONTENT

Supporting Information

The Supporting Information is available free of charge on the ACS Publications website at DOI: 10.1021/acs.jpcc.7b11671.

^{31}P and ^{1}H Hahn echo ssNMR spectra of probe background collected at 7.4 T at an MAS rate of 20 kHz and ^{1}H Hahn echo ssNMR spectra of probe background compared to ^{15}N-labeled NG collected at 11.7 T at an MAS rate of 15 kHz (PDF)

AUTHOR INFORMATION

Corresponding Author

*E-mail: goward@mcmaster.ca. Phone: 905-525-9140 ext. 26317.

ORCID

Kristopher J. Harris: 0000-0003-4205-7761
Zhongwei Chen: 0000-0003-3463-5509
Gillian R. Goward: 0000-0002-7489-3329

Author Contributions

The manuscript was written through contributions of all authors. All authors have given approval to the final version of the manuscript.

Notes

The authors declare no competing financial interest.

ACKNOWLEDGMENTS

Funding for this work was provided by the National Science and Engineering Research Council of Canada (NSERC), specifically through the Catalysis Research for Polymer Electrolyte Fuel Cell (CaRPE-FC) research network, as well as the Canada Research Chair (CRC) program, the Automotive Partnership of Canada (APC), McMaster University, the University of Waterloo, and the University of Western Ontario.

REFERENCES

(1) Carrette, L.; Friedrich, K. A.; Stimming, U. Fuel Cells—Fundamentals and Applications. *Fuel Cells* **2001**, *1*, 5−39.
(2) Carrette, L.; Friedrich, K. A.; Stimming, U. Fuel Cells: Principles, Types, Fuels, and Applications. *ChemPhysChem* **2000**, *1*, 162−193.
(3) Goodenough, J. B.; Park, K.-S. The Li-Ion Rechargeable Battery: A Perspective. *J. Am. Chem. Soc.* **2013**, *135*, 1167−1176.
(4) Jacobson, M. Z.; Delucchi, M. A. Providing All Global Energy with Wind, Water, and Solar Power, Part I: Technologies, Energy Resources, Quantities and Areas of Infrastructure, and Materials. *Energy Pol.* **2011**, *39*, 1154−1169.
(5) Winter, M.; Brodd, R. J. What Are Batteries, Fuel Cells, and Supercapacitors? *Chem. Rev.* **2004**, *104*, 4245−4270.
(6) Bockris, J. O. M.; Veziroglu, T. N. Estimates of the Price of Hydrogen as a Medium for Wind and Solar Sources. *Int. J. Hydrogen Energy* **2007**, *32*, 1605−1610.
(7) Connolly, D.; Lund, H.; Mathiesen, B. V. Smart Energy Europe: The Technical and Economic Impact of One Potential 100% Renewable Energy Scenario for the European Union. *Renew. Sustain. Energy Rev.* **2016**, *60*, 1634−1653.
(8) Lauber, V.; Jacobsson, S. The Politics and Economics of Constructing, Contesting and Restricting Socio-Political Space for Renewables—the German Renewable Energy Act. *Environ. Innov. Soc. Trans.* **2016**, *18*, 147−163.
(9) Nizami, A. S.; Shahzad, K.; Rehan, M.; Ouda, O. K. M.; Khan, M. Z.; Ismail, I. M. I.; Almeelbi, T.; Basahi, J. M.; Demirbas, A. Developing Waste Biorefinery in Makkah: A Way Forward to Convert Urban Waste into Renewable Energy. *Appl. Energy* **2017**, *186*, 189−196.
(10) Andor, M.; Voss, A. Optimal Renewable-Energy Promotion: Capacity Subsidies vs Generation Subsidies. *Resour. Energy Econ.* **2016**, *45*, 144−158.
(11) Susac, D.; Sode, A.; Zhu, L.; Wong, P. C.; Teo, M.; Bizzotto, D.; Mitchell, K. A. R.; Parsons, R. R.; Campbell, S. A. A Methodology for Investigating New Nonprecious Metal Catalysts for Pem Fuel Cells. *J. Phys. Chem. B* **2006**, *110*, 10762−10770.
(12) Qiao, J.; Xu, L.; Ding, L.; Zhang, L.; Baker, R.; Dai, X.; Zhang, J. Using Pyridine as Nitrogen-Rich Precursor to Synthesize Co-N-S/C Non-Noble Metal Electrocatalysts for Oxygen Reduction Reaction. *Appl. Catal. B Environ.* **2012**, *125*, 197−205.

(13) Xu, L.; Pan, G.; Shi, X.; Zou, C.; Zhou, Y.; Luo, G.; Chen, G. A Non-Noble Material Cathode Catalyst Dual-Doped with Sulfur and Nitrogen as Efficient Electrocatalysts for Oxygen Reduction Reaction. *Electrochim. Acta* **2015**, *177*, 57−64.
(14) Gong, K.; Du, F.; Xia, Z.; Durstock, M.; Dai, L. Nitrogen-Doped Carbon Nanotube Arrays with High Electrocatalytic Activity for Oxygen Reduction. *Science* **2009**, *323*, 760.
(15) Cruz-Silva, E.; López-Urías, F.; Muñoz-Sandoval, E.; Sumpter, B. G.; Terrones, H.; Charlier, J.-C.; Meunier, V.; Terrones, M. Electronic Transport and Mechanical Properties of Phosphorus-and Phosphorus−Nitrogen-Doped Carbon Nanotubes. *ACS Nano* **2009**, *3*, 1913−1921.
(16) Czerw, R.; Terrones, M.; Charlier, J.-C.; Blase, X.; Foley, B.; Kamalakaran, R.; Grobert, N.; Terrones, H.; Tekleab, D.; Ajayan, P. M. Identification of Electron Donor States in N-Doped Carbon Nanotubes. *Nano Lett.* **2001**, *1*, 457−460.
(17) Zhang, C.; Mahmood, N.; Yin, H.; Liu, F.; Hou, Y. Synthesis of Phosphorus-Doped Graphene and Its Multifunctional Applications for Oxygen Reduction Reaction and Lithium Ion Batteries. *Adv. Mater.* **2013**, *25*, 4932−4937.
(18) Ma, X.; Ning, G.; Qi, C.; Xu, C.; Gao, J. Phosphorus and Nitrogen Dual-Doped Few-Layered Porous Graphene: A High-Performance Anode Material for Lithium-Ion Batteries. *ACS Appl. Mater. Interfaces* **2014**, *6*, 14415−14422.
(19) Alam, T. M.; Friedmann, T. A.; Schultz, P. A.; Sebastiani, D. Low Temperature Annealing in Tetrahedral Amorphous Carbon Thin Films Observed by ^{13}C NMR Spectroscopy. *Phys. Rev. B Condens. Matter* **2003**, *67*, 245309.
(20) Cai, W.; Piner, R. D.; Stadermann, F. J.; Park, S.; Shaibat, M. A.; Ishii, Y.; Yang, D.; Velamakanni, A.; An, S. J.; Stoller, M.; et al. Synthesis and Solid-State NMR Structural Characterization of ^{13}C-Labeled Graphite Oxide. *Science* **2008**, *321*, 1815−1817.
(21) Liu, T.; Leskes, M.; Yu, W.; Moore, A. J.; Zhou, L.; Bayley, P. M.; Kim, G.; Grey, C. P. Cycling Li-O_2 Batteries Via LiOH Formation and Decomposition. *Science* **2015**, *350*, 530−533.
(22) Leskes, M.; Kim, G.; Liu, T.; Michan, A. L.; Aussenac, F.; Dorffer, P.; Paul, S.; Grey, C. P. Surface-Sensitive NMR Detection of the Solid Electrolyte Interphase Layer on Reduced Graphene Oxide. *J. Phys. Chem. Lett.* **2017**, *8*, 1078−1085.
(23) Blanc, F.; Leskes, M.; Grey, C. P. In Situ Solid-State NMR Spectroscopy of Electrochemical Cells: Batteries, Supercapacitors, and Fuel Cells. *Acc. Chem. Res.* **2013**, *46*, 1952−1963.
(24) MacIntosh, A. R.; Harris, K. J.; Goward, G. R. Structure and Dynamics in Functionalized Graphene Oxides through Solid-State NMR. *Chem. Mater.* **2015**, *28*, 360−367.
(25) Harris, K. J.; Bugnet, M.; Naguib, M.; Barsoum, M. W.; Goward, G. R. Direct Measurement of Surface Termination Groups and Their Connectivity in the 2D Mxene V_2CT_X Using NMR Spectroscopy. *J. Phys. Chem. C* **2015**, *119*, 13713−13720.
(26) Harris, K. J.; Reeve, Z. E. M.; Wang, D.; Li, X.; Sun, X.; Goward, G. R. Electrochemical Changes in Lithium-Battery Electrodes Studied Using ^{7}Li NMR and Enhanced ^{13}C NMR of Graphene and Graphitic Carbons. *Chem. Mater.* **2015**, *27*, 3299−3305.
(27) Liu, H.; Liu, Y.; Zhu, D. Chemical Doping of Graphene. *J. Mater. Chem.* **2011**, *21*, 3335−3345.
(28) Wang, H.; Maiyalagan, T.; Wang, X. Review on Recent Progress in Nitrogen-Doped Graphene: Synthesis, Characterization, and Its Potential Applications. *ACS Catal.* **2012**, *2*, 781−794.
(29) Usachov, D.; Vilkov, O.; Grüneis, A.; Haberer, D.; Fedorov, A.; Adamchuk, V.; Preobrajenski, A.; Dudin, P.; Barinov, A.; Oehzelt, M. Nitrogen-Doped Graphene: Efficient Growth, Structure, and Electronic Properties. *Nano Lett.* **2011**, *11*, 5401−5407.
(30) Hummers, W. S.; Offeman, R. E. Preparation of Graphitic Oxide. *J. Am. Chem. Soc.* **1958**, *80*, 1339.
(31) Wagner, C. D. *The NIST X-ray Photoelectron Spectroscopy (XPS) Database*; US Department of Commerce, National Institute of Standards and Technology, 1991.
(32) Bertani, P.; Raya, J.; Bechinger, B. ^{15}N Chemical Shift Referencing in Solid State NMR. *Solid State Nucl. Magn. Reson.* **2014**, *61*−*62*, 15−18.
(33) Matthews, P. D.; King, T. C.; Glass, H.; Magusin, P. C. M. M.; Tustin, G. J.; Brown, P. A. C.; Cormack, J. A.; García-Rodríguez, R.; Leskes, M.; Dutton, S. E. Synthesis and Extensive Characterisation of Phosphorus Doped Graphite. *RSC Adv.* **2016**, *6*, 62140−62145.
(34) Bytchkov, A.; Fayon, F.; Massiot, D.; Hennet, L.; Price, D. L. ^{31}P Solid-State NMR Studies of the Short-Range Order in Phosphorus−Selenium Glasses. *Phys. Chem. Chem. Phys.* **2010**, *12*, 1535−1542.
(35) Lange, S.; Schmidt, P.; Nilges, T. Au_3SnP_7@ Black Phosphorus: An Easy Access to Black Phosphorus. *Inorg. Chem.* **2007**, *46*, 4028−4035.
(36) Nicholls, R. J.; Aslam, Z.; Sarahan, M. C.; Sanchez, A. M.; Dillon, F.; Koós, A. A.; Nellist, P. D.; Grobert, N. Morphology−Composition Correlations in Carbon Nanotubes Synthesised with Nitrogen and Phosphorus Containing Precursors. *Phys. Chem. Chem. Phys.* **2015**, *17*, 2137−2142.
(37) Harris, R. K.; Thompson, T. V.; Norman, P. R.; Pottage, C.; Trethewey, A. N. High-Resolution ^{2}H Solid-State NMR of $2H_2O$ Adsorbed onto Activated Carbon. *J. Chem. Soc., Faraday Trans.* **1995**, *91*, 1795−1799.
(38) Harris, R. K.; Thompson, T. V.; Norman, P. R.; Pottage, C. Adsorption Competition onto Activated Carbon, Studied by Magic-Angle Spinning NMR. *J. Chem. Soc., Faraday Trans.* **1996**, *92*, 2615−2618.
(39) Harris, R. K.; Thompson, T. V.; Forshaw, P.; Foley, N.; Thomas, K. M.; Norman, P. R.; Pottage, C. A Magic-Angle Spinning NMR Study into the Adsorption of Deuterated Water by Activated Carbon. *Carbon* **1996**, *34*, 1275−1279.
(40) Ramsey, N. F. Magnetic Shielding of Nuclei in Molecules. *Phys. Rev.* **1950**, *78*, 699.
(41) Park, S.; Hu, Y.; Hwang, J. O.; Lee, E.-S.; Casabianca, L. B.; Cai, W.; Potts, J. R.; Ha, H.-W.; Chen, S.; Oh, J. Chemical Structures of Hydrazine-Treated Graphene Oxide and Generation of Aromatic Nitrogen Doping. *Nat. Commun.* **2012**, *3*, 638.
(42) Harris, R. K.; Thompson, T. V.; Norman, P. R.; Pottage, C. Phosphorus-31 NMR Studies of Adsorption onto Activated Carbon. *Carbon* **1999**, *37*, 1425−1430.
(43) Gan, Z. $^{13}C/^{14}N$ Heteronuclear Multiple-Quantum Correlation with Rotary Resonance and Redor Dipolar Recoupling. *J. Magn. Reson.* **2007**, *184*, 39−43.
(44) Wang, X.; Hou, Z.; Ikeda, T.; Terakura, K. NMR Chemical Shifts of 15n-Bearing Graphene. *J. Phys. Chem. C* **2014**, *118*, 13929−13935.
(45) Stone, A. J.; Wales, D. J. Theoretical Studies of Icosahedral C^{60} and Some Related Species. *Chem. Phys. Lett.* **1986**, *128*, 501−503.

DOI: 10.1021/acs.jpcc.7b11671
J. Phys. Chem. C 2018, 122, 6593−6601